Comparative analysis of direct (core) and indirect (borehole imaging tools) collection of fracture data in the Hot Dry Rock Soultz reservoir (France)

Albert Genter, C. Castaing, Chrystel Dezayes, H. Tenzer, Hervé Traineau, T. Villemin

JOURNAL OF GEOPHYSICAL RESEARCH, VOL. 102, NO. B7, PAGES 15,419–15,431, JULY 10, 1997

Comparative analysis of direct (core) and indirect (borehole imaging tools) collection of fracture data in the Hot Dry Rock Soultz reservoir (France)

A. Genter,[1] C. Castaing,[1] C. Dezayes,[2] H. Tenzer,[3] H. Traineau,[1] and T. Villemin[2]

Abstract. Attributes of several thousand fractures were collected in three boreholes of 2.2, 3.6, and 3.8 km depth, penetrating the Soultz Hot Dry Rock reservoir (France). The fractures were sampled from cores and from several high-resolution imaging techniques such as borehole televiewer (BHTV), ultrasonic borehole imager (UBI), formation microscanner (FMS), formation microimager (FMI), and azimuthal resistivity imaging (ARI). A comparison was made between the data collected on cores and those provided by different imaging techniques. The comparison clearly establishes that the different wall- images are not as exhaustive as the core data and cannot provide a complete characterization of the fracture network. Discrete fractures thinner than 1 mm are not properly detected. This is also the case for discrete fractures closer than 5 mm, which appear only as single traces. The imaging techniques are, nevertheless, very powerful for characterizing altered fracture clusters. Whatever the technique used, the fracture strikes were correctly sampled with the different systems. This comparison allowed us to calibrate the fracture population data obtained from the imaging system in order to correct for the filtering effect introduced by the technique itself and by the alteration of the rock mass.

Introduction

Knowledge of the spatial distribution of fractures at depth has great economic significance, since they can create highly anisotropic permeability within petroleum or geothermal reservoirs or cause engineering problems in nuclear- waste repository sites. For such applications, the fractured rock mass must be investigated by deep wells, and the quantitative characterization of the fracture system is determined as soon as possible during drilling, using core samples and/or borehole imagery. However, because continuous coring is becoming more and more expensive, fracture characterization tends to be obtained from borehole imagery only. Consequently, the obtained fracture data are less detailed than would be the case from core analysis [*Genter et al.*, 1995]. So far, few attempts have been made to evaluate the reliability of borehole imaging in characterizing fractured reservoirs in granite or clastic formations. The Soultz Hot Dry Rock (HDR) test site at Soultz-sous-Forêts (Rhine graben, France), where three adjacent wells (EPS1, GPK1, and GPK2) intersect the same sandstone formation and granite, is suitable for making detailed comparisons between core and image data because fracture attributes, such as orientation, spacing, density, and thickness, were systematically collected on continuous core sections in one well and acoustic or electrical imaging was carried out in all three wells. Here we compare the fracture population observed on cores directly with the fracture population interpreted from borehole images, so that in the future it will be possible to derive fracture characteristics from borehole imagery only.

Geological Setting of the Hot Dry Rock Site

The Rhine graben, which extends for 300 km in the north-northeast direction between Basel and Frankfurt [Ziegler, 1992], can be considered as one of the best-documented basins in the West European rift system since its deep structure is well known through extensive recent geophysical work [Wenzel et al., 1991; Brun et al., 1991, 1992]. The three major geological events that structured this area are the Variscan orogeny, the subsequent late-tectonic extension, and the Cenozoic opening of the Rhine graben rift system.

The Soultz Hot Dry Rock site, which is located within the Upper Rhine valley (France) approximately 6 km from the major fault bordering the graben to the west (Figure 1a), has been dedicated to extensive geothermal research involving British, French, and German scientific teams. It corresponds to a local horst structure within the Rhine graben, bounded by north trending faults dipping either west or east. The objective of the HDR project is to develop an experimental deep thermal exchanger in a granite basement that is covered by 1400 m of Triassic to Tertiary sediments [Kappelmeyer et al., 1991; Elsass et al., 1995]. Since 1987, two reconnaissance wells (EPS1 and GPK1 (Figure 1b)) lying 500 m apart have been drilled to 2230 and 3600 m, respectively, in the granite basement. In 1995, a new well (GPK2) was drilled to 3880 m for planned interwell circulation tests with GPK1 [Baria et al., 1995]. Extensive well testing in GPK1 has characterized the fracture system down to 3600 m in the granitic basement

[1]Département Géophysique et Imagerie Géologique, Direction de la Recherche, Bureau de Recherches Géologiques et Minières, Orléans, France.
[2]Laboratoire Géodynamique des Chaînes Alpines, Université de Savoie, Le Bourget de Lac, France.
[3]Stadtwerke Bad Urach, Bad Urach, Germany.

Paper number 97JB00626.
0148-0227/97/97JB-00626$09.00

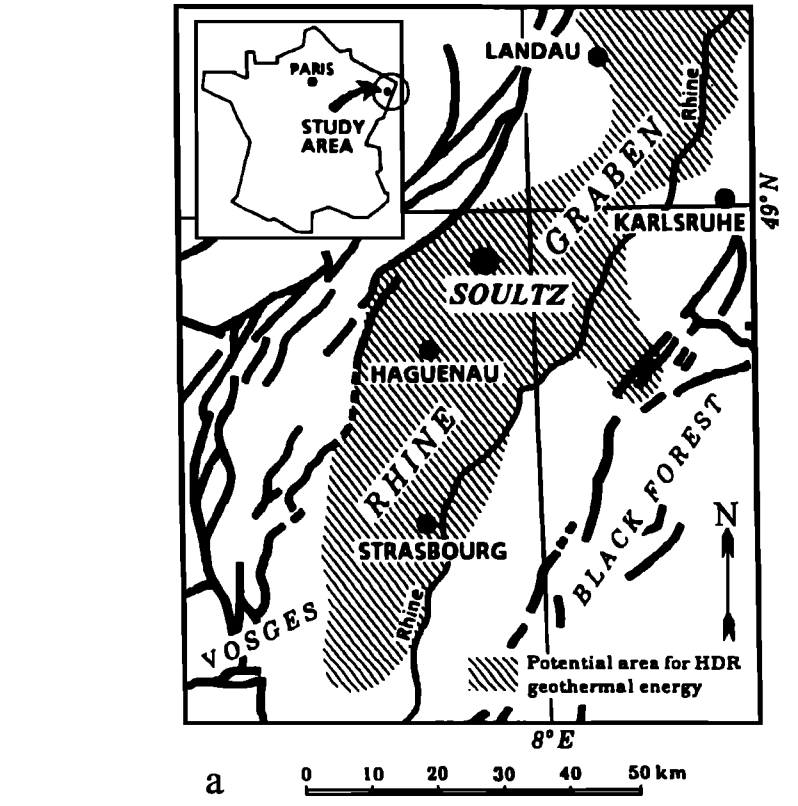

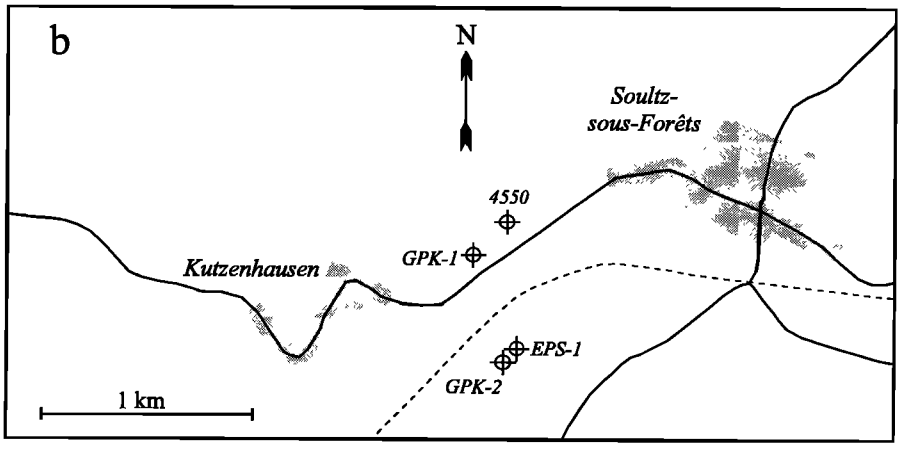

Figure 1. (a) Site location and (b) well distribution at the Soultz Hot Dry Rock test site.

which supports a natural convective flow [Jung et al., 1995], giving rise to temperatures of about 110°C at the top of the granite but rather low gradients at greater depth [Garnish et al., 1994]. Temperatures in well GPK1 are 140°C at 2000 m and 160°C at 3590 m depth [Schellschmidt and Schulz, 1991]. Variations in the thermal gradient suggest that there is a zone of enhanced permeability above the interface between the granite and the sedimentary cover, supporting the upper portion of a convection cell penetrating at least to 3500 m into the granite [Flores and Royer, 1992; Garnish et al., 1994; Le Carlier et al., 1994; Benderitter et al., 1995].

Data Analysis

Cores and Borehole Images

The data available from wells EPS1, GPK1, and GPK2 are not equivalent in terms of physical measurements. For well EPS1, which is an exploratory slim hole, both acoustic imagery data sampled by the borehole televiewer (BHTV), facsimile tool from Deutsche Montan Technologie (DMT) and continuous cores are available. Owing to the high quality of the coring, with recovery close to 100% [*Genter and Traineau*, 1992], well EPS1 can be considered as a reference

well for calibrating the geological features of the granite recorded on the cores and their physical properties revealed by the borehole imaging. For well GPK1, which is a production well, coring was very limited (less than 50 m) and only represents about 2% of the total drilled length. However, this well does provide 2200 m of continuous high-resolution borehole electrical imagery (formation microscanner (FMS) and formation microimager (FMI) from Schlumberger) and 700 m of low-resolution azimuthal resistivity measurements (azimuthal resistivity imaging (ARI) from Schlumberger) in the deeper part of the well. BHTV data were continously recorded between 1376 and 3600 m depth. For well GPK1, a new borehole televiewer (ultrasonic borehole imager (UBI) from Schlumberger) provided 655 m of high-resolution acoustic measurements. Finally, for well GPK2, which is an injection well, no coring was carried out, but the UBI televiewer provided 2400 m of high-resolution acoustic measurements.

Well EPS1 was fully cored through the Lower Triassic sandstone (1000 m to 1420 m) and into the granite (1420 m to 2230 m) [*Genter and Traineau*, 1992], and BHTV data were obtained in the same depth interval, providing a rugosity map of the whole borehole surface. The BHTV (DMT) is a borehole acoustic logging tool in which an ultrasonic pulse is emitted by a rotating transducer and reflected from the borehole wall [*Zemanek et al.*, 1970]. It uses a single piezoelectric 1.3 MHz transducer, which acts as a source and also as a receiver for the reflected signal at the borehole wall. The rotating beams scans the rock mass at a rate of three returns per second, transmitting pulses 256 times per cycle; both amplitude of the reflected beam and transit time are measured. The vertical resolution is directly linked to the logging speed and in well EPS1 is about 5 mm, obtained from a very slow logging speed of 61 m per hour. Because of the occurrence of near-vertical fractures, it is also important to know horizontal resolution; here with a well diameter of 12.7 cm, the pulse rate of 256 revolutions gives a peripherical resolution of 1.5 mm. The fractures were analyzed manually on the BHTV images by a superimposition of overlays [*Tenzer et al.*, 1992]. The UBI tool uses a high-resolution focused open hole transducer. The UBI was used in wells GPK1 and GPK2 with a 500-kHz frequency which provided a high horizontal resolution of 5 mm [*Schlumberger*, 1993]. The recommended logging speed of 244 m per hour gives a vertical resolution (sampling rate) of 10 mm.

Well GPK1 was drilled first to 2000 m in 1987 and then deepened to 3600 m in 1993. For the upper section (1420 m to 2000 m), BHTV and FMS data were collected and analyzed by *Tenzer et al.* [1991] and *Genter et al.* [1991], respectively. With the FMS-4 pads version used in this study, about 50% of the borehole wall was imaged to obtain an oriented picture of the borehole wall by mapping its electrical conductivity, using an array of small, pad-mounted electrodes [*Ekstrom et al.*, 1986; *Luthi and Banavar*, 1988]. The sensors are distributed azimuthally on a conducting pad and every 2.54 mm (0.1 inch) record a series of microresistivity curves. During logging, a current flows from each sensor to a single return electrode located at the top of the sonde. The current intensity data, which represent the microresistivity variations of the borehole surface, are converted to variable-intensity gray or color pictures. In this way, high-resistivity zones appear white, and low-resistivity zones appear dark. In crystalline rock such as the Soultz granite, a conducting fracture can be detected as a dark anomaly mark on the image. The sampling rate of the FMS is about 3 mm and corresponds to its vertical resolution. The horizontal resolution related to the pad configuration is 7.5 mm [*Schlumberger*, 1992], but the tool is able to detect thinner features if these have a sufficiently high resistivity contrast [*Ekstrom et al.*, 1986; *Pezard et al.*, 1992]. *Genter et al.* [1991] used a specific software developed on the Schlumberger Formation Image Examiner workstation [*Boyeldieu and Jeffreys*, 1988; *Bourke et al.*, 1989] to interpret the image data and analyze the natural fracture network encountered in the GPK1 well between 1420 m and 2000 m depth. For the deeper section of well GPK1 (2000 m to 3600 m), the BHTV data are accompanied by FMI data. The FMI is a new version of the geoelectrical imagery tool combining high-resolution measurements (horizontal resolution 5 mm) with full bore coverage. The FMI images were interpreted [*Genter et al.*, 1995] using the FMI image software which is a new version of the BHTV image interactive workstation [*Barton et al.*, 1991].

The 15.87 cm-section of well GPK1 (2780 m to 3500 m) was also logged by ARI, and the interpretation was compared with the FMI results [*Genter and Genoux-Lubain*, 1994]. This new generation of electrical imager is a standard laterolog equipped with an additional segmented electrode which provides 12 deep calibrated azimuthal resistivity measurements [*Davies et al.*, 1992; *Faivre*, 1993]. In a 15.2- to 20.3-cm-diameter borehole, the vertical resolution of the ARI is of the order of 200 mm, whereas its horizontal resolution is about 45 mm. Although it has much lower spatial resolution than the FMS and FMI imagers, it is able to characterize fracture over a certain distance which is relevant to fluid flow. The deepest section in well GPK1 (between 2850 and 3505 m depth) was logged with the UBI, and the data were depth matched with FMI data.

Well GPK2 was drilled to a depth of 3880 m in 1995. High-resolution acoustic data (UBI) were collected between 1420 and 3800 m and then interpreted in terms of fractures [*Genter et al.*, 1996] by using the BHTV image software [*Barton et al.*, 1991].

Hole conditions were fairly similar during logging operations with all the borehole imaging techniques used at Soultz. The different near-vertical holes all penetrated the same granite rock and were filled with clean salty water.

Fracture Orientation

The accuracy of fracture orientations determined from borehole images can be considered as the sum of the errors from the different stages of data analysis. Error may first be introduced by the tool inclinometry system, and a second error may depend on the technique of dip picking, that is, manually using sinusoid overlay or using computerization. The accuracy of the magnetometers is of the order of ±2° on dip azimuth and ±0.2° on dip magnitude [*Schlumberger*, 1986] if the rock is not too magnetic. Concerning hand-measured dips on the BHTV grey-scale paper log, the errors inherent to this procedure are estimated to be typically of the order of ±5°. Interactively picked data from FMS or FMI images, using a workstation to provide dip information, have

Table 1. Data Collection of Natural Fractures in Wells EPS1, GPK1, and GPK2

Well	Lithology	Depth Interval	Data Collection	Measured Fractures	Oriented Fractures	Fracture Density fracture/m
EPS1	Sandstone	1000-1420 m	Core	348	322	0.83
			BHTV	177	177	0.42
	Granite	1420-2230 m	Core	3055	2997	3.77
			BHTV	517	517	0.64
	Massive granite		Core		698	1.24
			BHTV	340	340	0.60
	Altered granite		Core		2309	9.07
			BHTV	177	177	0.70
GPK1	Granite	1420-2000 m	FMS	483	483	0.83
		2000-3600 m	FMI	593	593	0.37
		2780-3500 m	ARI	233	202	0.33
		1376-3600 m	BHTV	1380	1380	0.63
	Granite	1376-2000 m	BHTV	714	714	1.15
	Granite	2000-3600 m	BHTV	666	666	0.42
	Granite	2850-3505 m	UBI	500	500	0.76
GPK2	Granite	1420-3800 m	UBI	1792	1792	0.75

an excellent azimuth accuracy [*Bourke*, 1992; *MacLeod et al.*, 1990].

The main sources of error thus arise from the ability of the interpreter to pick dip planes consistently. *Bourke* [1992] describes a series of tests from FMS data performed on the same bed boundaries within a cross-bedded sequence. The reproducibility error is ±2°-3° on dip magnitude and ±6°-8° on dip azimuth. In well EPS1, the strikes of the fractures observed on cores were determined by digitizing their sinusoid trace on a flat core copy to ±5° [*Genter and Traineau*, 1992]. Furthermore, core data orientation introduces an additional 5° of uncertainty in comparison to BHTV images. All considered, the values of ±15° and ±5° for dip-azimuth and dip-magnitude errors, respectively, can be considered as reasonable estimations.

Fracture Typology

The fracture population discussed in this paper only relates to naturally formed fractures and excludes drilling-induced fractures. The fracture data sets collected in wells EPS1, GPK1, and GPK2 are given in Table 1. Thus for well EPS1, the strike, dip, and spacing of 3403 fractures were recorded from the cores and compared to the 694 fractures (only) observed on the BHTV images over the same depth interval. For well GPK1, the strike, dip, and spacing of 1380 fractures collected from the BHTV were compared to the results of the UBI, FMS, FMI, and ARI images. Finally, for well GPK2, the strike, dip, and spacing of 1792 fractures were determined from the UBI images.

Structural analysis of the core samples has defined several fracture types in sandstone and granite: subhorizontal joints, steeply dipping filled- joints, and steeply dipping filled-sealed faults [*Genter and Traineau*, 1996]. The subhorizontal joints correspond to sheet- joints caused by unloading [*Engelder*, 1987; *Pollard and Aydin*, 1988]. The steeply dipping filled-joints are minor mode I discontinuities filled by hydrothermal products. The steeply dipping faults were commonly sealed during several hydrothermal stages, and they may exhibit slight to prominent wall- rock alteration including argillization. These faults originated as filled- joint planes that were reactivated into mode II shear fractures, as indicated by striation marks and slickensides that show normal, reverse, sinistral, or dextral slips. Some of the sealed- faults with a thick hydrothermal filling show a free residual aperture due to incomplete sealing. This fracture typology is valid for both sandstone and granite, except for the subhorizontal joints which only occur within the granite. To complete the fracture typology, some clastic dikes filled with fine-grained sandstone material observed in the Triassic sandstone are interpreted as synsedimentary fractures. Unfortunately, it has not been possible to distinguish the above fracture types from borehole imagery alone, and consequently, all the determined planar discontinuities have been called fractures.

Fracture Determination in Well EPS1

The fractures in well EPS1 interpreted from the BHTV imagery could be compared directly with the natural fractures measured on the cores.

Fracture Density

Figure 2 shows the cumulative number of fractures versus depth determined from 1000 m to 2230 m and obtained from both core and BHTV. The plot shows an increasing fracture density with depth, the slope of the curve being proportional to the rate of increase; that is, the lower the slope is, then the higher the number of fractures encountered along the borehole is. Within the sandstone, the two curves representing core and BHTV data are almost parallel and show regular trajectories with depth; these correspond to a fairly low increase in fracture density with depth (BHTV, 0.42 fractures/m and core, 0.83 fractures/m). Once within the granite, the results from core and BHTV are totally different. The BHTV data show a slight and regular fracture density (0.64 fractu-

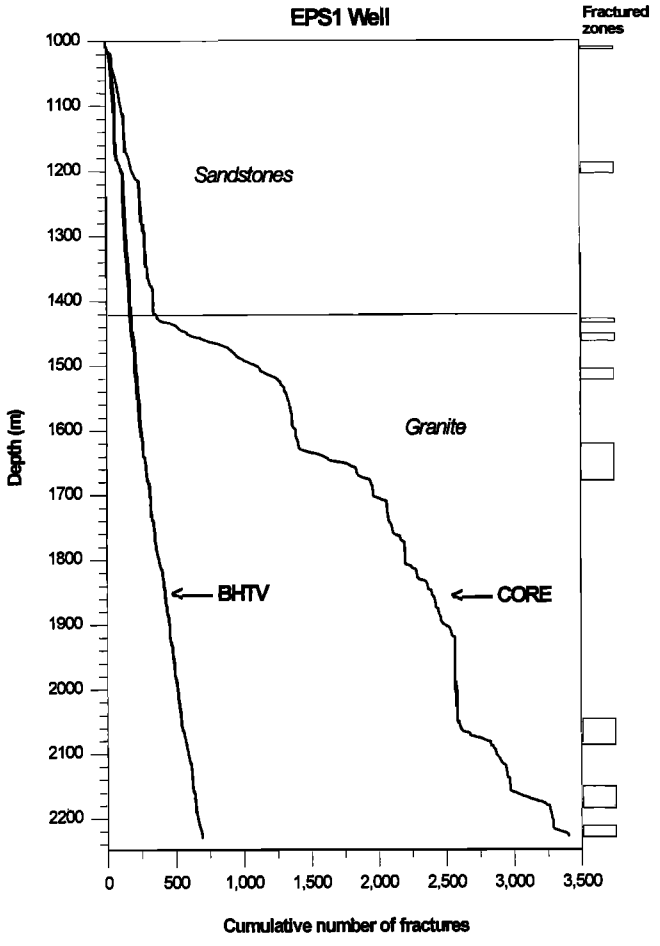

Figure 2. Cumulative number of fractures versus depth over the interval 1000-2230 m for both core and borehole televiewer (BHTV) data collected in well EPS1. Fractured zones were determined from both core examination and BHTV interpretation.

res/m), whereas the core data show a higher and chaotic fracture density increase (3.77 fractures/m on average): low-fracture intervals (1520 to 1620 m and 1910 to 2040 m with 0.7 to 1.3 fractures/m, respectively, on average) coexist with high-fracture intervals (1770 m to 1840 m with 4.0 fractures/m on average) and also with intense-fracture zones (1420 to 1460 m, 1620 to 1660 m, 2050 to 2080 m, and 2150 to 2180 m with 9.0 fractures/m on average). The intense-fracture zones correlate with fault zones that developed hydrothermal alteration [*Genter et al.*, 1995], and low-fracture intervals correspond to massive unaltered granite. The BHTV thus has a filtering effect on fracture detection, this is less important in the sandstone where 50% of the fractures are recorded, than in the granite where only 17% of the fractures were recorded. This selectivity can be analyzed in relation to the main petrographic zones within the granite, that is, the unaltered massive zones and the hydrothermally altered fractured zones. The ratio of fracture numbers recorded from BHTV and core is around 50% within the unaltered massive granite, as opposed to only 5% in the altered and fractured zones (Table 1). The better BHTV fracture-detection rate in massive granite could be related to the fact that the high cohesion of the massive rock induces a low borehole wall roughness, whereas altered and fractured zones impart too high a wall roughness for good acoustic signal recording.

Two examples of core and BHTV fracture characterization are presented on Figure 3. Figure 3a shows a cluster of small-scale fractures in the Triassic sandstone, sampled at about 1173 m depth and visible on both core and the BHTV image. The fact that fractures were recorded both in transit time and in amplitude signal suggests that they are slightly open, which was confirmed by the core analysis. On the core, the fractures present a significant residual free aperture and a 1- to 10-mm-thick sealed-barite infill. Figure 3b shows a cluster of near-vertical fractures sampled in the sandstone at 1214 m depth and visible on the core but not on the BHTV image. Here the core analysis showed that the fractures present a thinner sealed width (less than 1 mm) and that only the fracture detected by the BHTV has a significant free aperture. As fractures having a sealed width of less than 1 mm represent 45% of the total amount of core-sampled fractures in the Triassic sandstone, the fact that BHTV detects about 50% of the total amount of fractures in sandstone (Table 1) gives an idea of its resolution, that is, between 1 and 2 mm. In the granite, core analysis showed that 75% of the fractures are less than 1 mm- thick [*Genter and Traineau*, 1996], which could explain why 83% of the fractures were not recorded by the BHTV in the granite. As mentioned by *Barton and Zoback* [1992], it is possible that the small fractures are below the size of BHTV resolution and thus would not be detected regardless of the quality of the granite. Between 1910 and 2050 m, which corresponds to a very slightly altered and fractured section (Figure 2), 0.62 fractures/m were detected with the BHTV as opposed to 0.24 fractures/m on the core. It could appear that the overestimation of the BHTV-recorded fractures in this interval could be due to the occurrence of drilling-induced fractures which were not taken into account in core analysis. This fact enhances the difficulty in clearly separating natural and drilling-induced fractures when interpreting borehole imagery.

Fracture Orientation

Although fracture orientation in the Soultz wells has already been discussed in previous papers [*Genter et al.*, 1991, 1995; *Dezayes et al.*, 1995], no detailed comparison has been made between BHTV image and core data. The EPS1 cores in the Triassic sandstone show two major fracture sets trending N-S to NNW-SSE (N0° 75°W and N165° 75°E). These two main sets are close to a conjugate fracture pattern of normal faults related to the formation of the Rhine graben. Two minor sets trending NW-SE (N120° 75°N) and NE-SW (N050° 75°N) are associated with the principal N-S trending fracture sets (Figure 4a). The BHTV data show approximately the same major set trending N-S (N170° 75°W and N0° 70°E) and the same minor sets trending NW-SE (N120° 75°S) and NE-SW (N30° 70°W and N30° 70°E) (Figure 4b). Consequently, there is good agreement between core and BHTV data for fracture orientation within the sandstone, the only differences is in the relative percentage of fractures within the different sets.

In the granite, the EPS1 cores show the two major fracture sets trending N-S (N0° to N40° 80°W and N170° 70°E) (Figure 4c). The BHTV data gives one major set trending NE-SW (N45° 80°W) which is associated with two minor sets trending N-S (N0° 80°W and N170° 65°E) and E-W (N100°

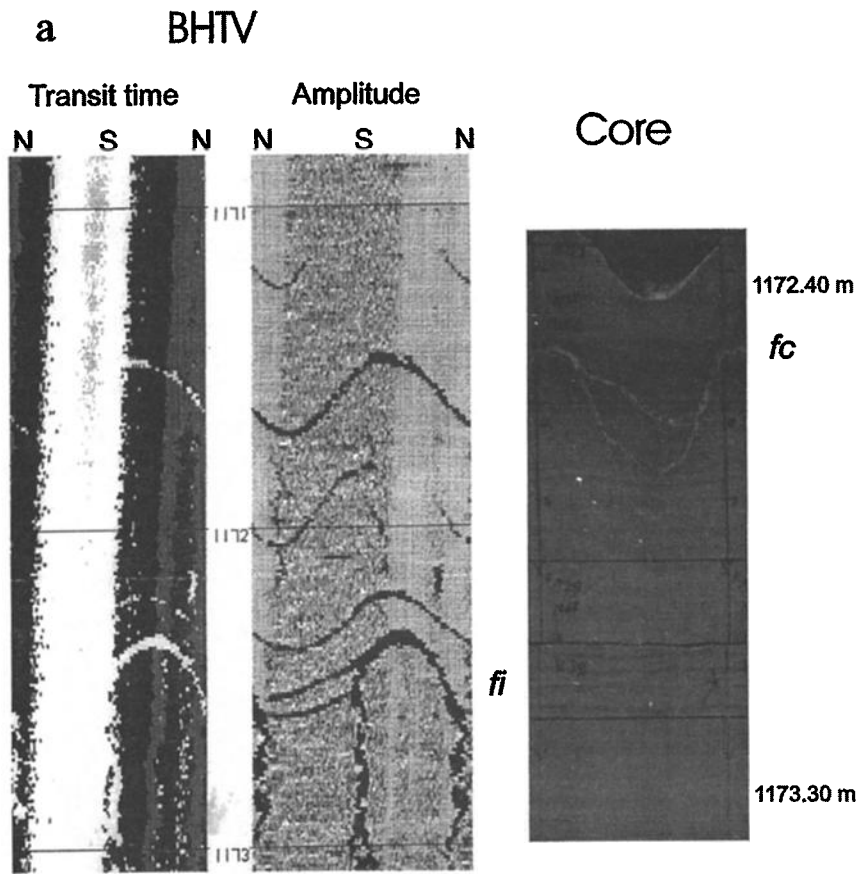

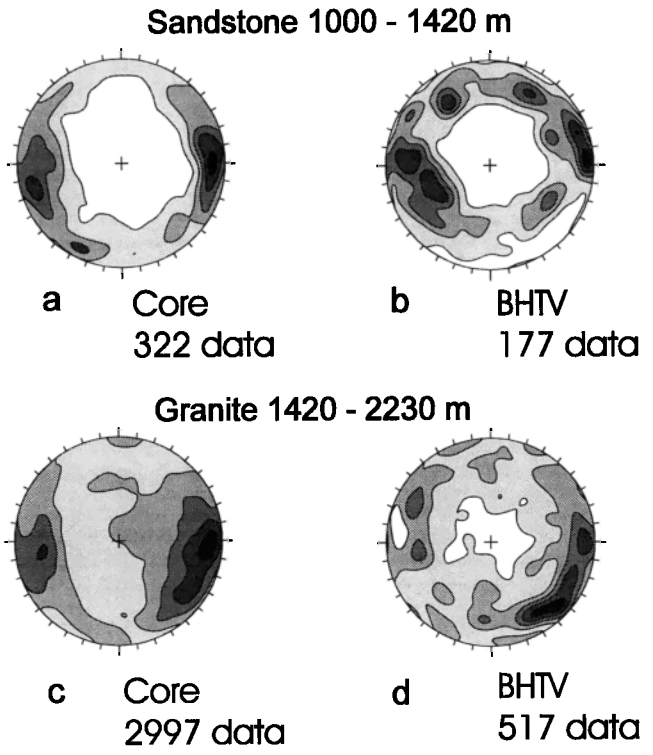

Figure 4. Schmidt isodensity projection (lower- hemisphere) of the pole of natural fractures observed (a) on the core and (b) on BHTV in the sedimentary section of well EPS1 and (c) on the core and (d) on BHTV in the granitic section of well EPS1. The different contours indicate 10%, 30%, 50%, and 90% of the whole fracture population.

75°N) (Figure 4d). The agreement between core and BHTV data is not as good as in the sandstone because of the fact that the relative percentage of fractures within the various sets differs perceptibly. On the BHTV images, the N-S trending sets are less marked, and the E-W trending set is more marked than in the core data.

The same comparison was also carried out after separating the massive and the hydrothermally altered and fractured zones in the granite (Figure 5). In the massive zones, the fracture directions are fairly similar in both the core and BHTV data, apart from the N100°-oriented fracture set which is only found on the BHTV images (Figures 5a and 5b), albeit that the NE-SW and NW-SE fracture sets are better documented on BHTV images than on the core sections. In the altered and fractured zones, the NNE-SSW and NNW-SSE-oriented fracture sets are the same with both core and BHTV data; here the discrepancies come from the fact that the NE-SW and E-W- oriented sets are extremely well expressed on the BHTV images (Figures 5c and 5d).

At Soultz therefore the BHTV gives a better estimation in fracture detection in massive granite, where the physical constrasts are higher, than in hydrothermally altered and fractured granite where less than 8% of discrete fractures were detected. It must also be noted, in relation to fracture orientation, that the BHTV estimation is better in the sandstone than in the granite, owing to the high rate of fracture detection (Figures 2 and 3a and 3b).

Fracture Spacing

Cumulative distributions of fracture spacings plotted on log/log graphs can show power- law (or fractal) distributions evidenced by straight lines or exponential and lognormal distributions forming convex-upward curves [*Gillespie et al.*, 1993].

In the Triassic sandstone, the cumulative fracture spacing distributions derived from both core and BHTV (Figure 6a) follow approximately the same negative exponential law for spacings greater than 0.8 m, but spacings less than 0.8 m are strongly underestimated; the closest fractures form clustered zones in which discrete fractures cannot properly be detected because of the limited resolution of the BHTV and the thinness of fracture seals that are probably below this resolution. In the granite, the fracture spacing distribution differs in the core and in the BHTV data (Figure 6b). The distribution derived from the core follows a power law with a breakdown in self-similarity for spacings greater than 3 m, whereas the distribution derived from the BHTV follows an exponential law. The minimum fracture spacing derived from BHTV is 5 mm (Figure 6b), and thus closest discrete fractures could appear as single traces.

Conclusions

Comparison between the core and the BHTV data in well EPS1 at Soultz shows that the BHTV introduces biases in characterizing fracture attributes such as density, orientation, and spacing of discrete fractures and that these biases are higher in the granite than in the Triassic sandstone. However, if we consider each fracture cluster as a single altered zone, then the BHTV is able to correctly detect these altered zones without differentiating each fracture. This comparison could lead to a definition of correcting factors that depend on the lithology, the state of fracturing, and the alteration of the rock mass. In the above example, the fracture density derived from BHTV data should be multiplied by around 2 for the sandstone and massive granite and by around 13 for the altered granite.

Figure 3. Examples of well EPS1 fractures visible both in full-oriented BHTV and in unrolled core photographs in well EPS1. BHTV data are presented in transit time and amplitude on 360° in logging depth reference; core data are presented on 360° in driller depth reference. (a) Fractures in sandstone at approximately 1173 m depth. A cluster of thin fractures (*fc*) is visible on both the unrolled core photograph and on the BHTV image. The individual fractures (*fi*) collected here are slightly open and well imaged by the BHTV technique. (b) Cluster of thin fractures in sandstone at approximately 1214 m depth. Thin fractures (*fc*) are visible on the unrolled core photograph, whereas only a fracture (*fi*), which is open, is imaged by the BHTV technique.

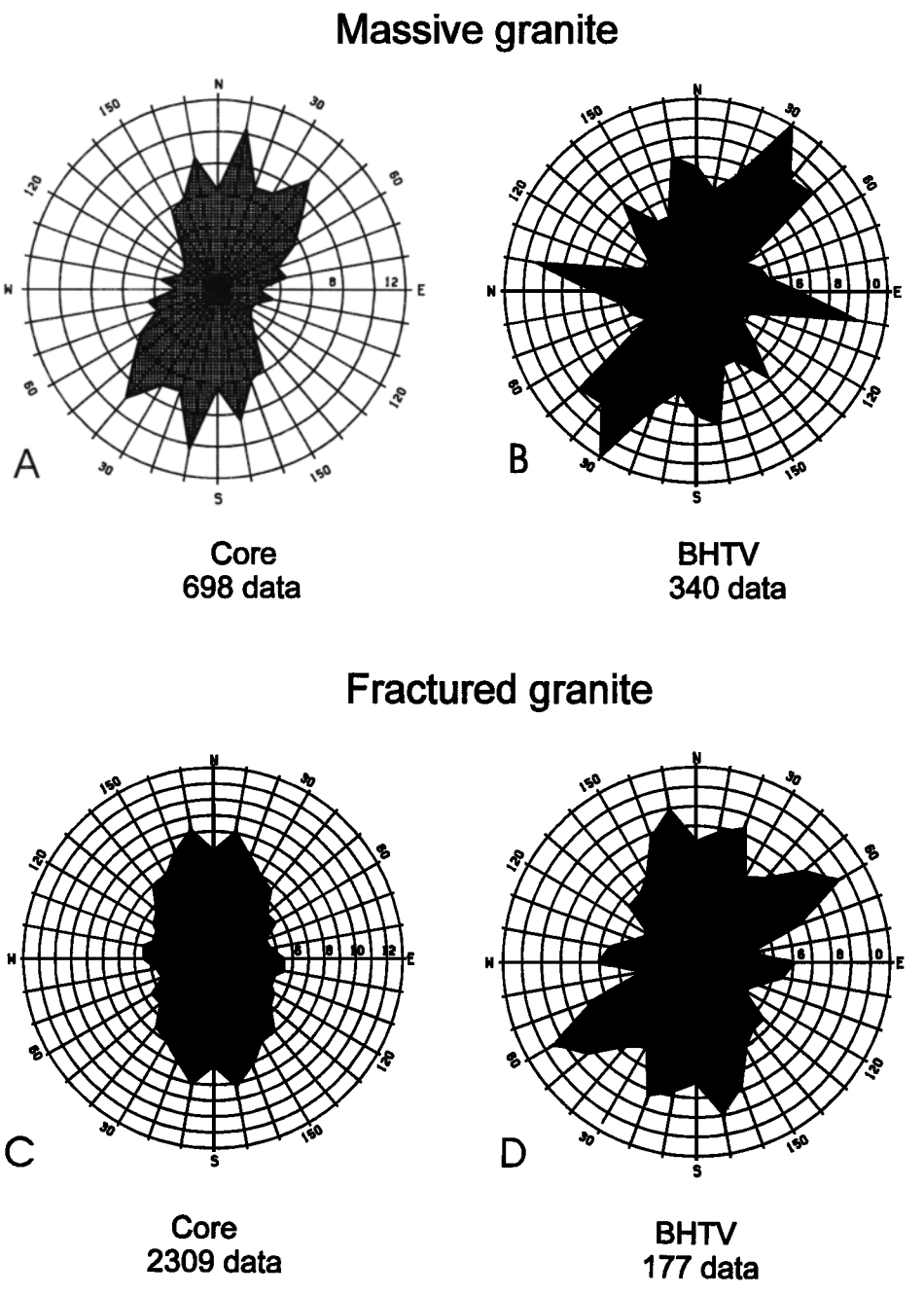

Figure 5. Rose diagrams of natural fracture strikes observed (a) on the core and (b) on BHTV in the massive granite of well EPS1 and (c) on the core and (d) on BHTV in altered granite in well EPS1.

Fracture Determination in Well GPK1

Fracture Density

Well GPK1, located 500 m to the north-northwest of well EPS1, was not fully cored but was logged with the BHTV and UBI acoustic tools and the FMS, FMI, and ARI electrical tools. This allowed us to compare the results of these different borehole imaging techniques from 1410 m to 3600 m in the granite.

Figure 7 shows the distribution of the cumulative number of fractures versus depth obtained in the granite from the different imageries: BHTV from 1376 to 3600 m, UBI from 2850 to 3505 m, FMS from 1420 to 2000 m, FMI from 2000 to 3600 m, and ARI from 2780 to 3500 m. The curves shows regular trajectories with a change in slope around 1900-2000 m. The FMS detected about 0.83 fractures/m down to 2000 m, and the FMI and ARI detected about 0.37 and 0.33 fractures/m, respectively. The FMI resolution being higher than the FMS resolution, the lower fracture density recorded by the FMI below 1900-2000 m depth cannot be assigned to the change in imaging tool. This is confirmed by the fact that the BHTV collected about 1.15 fractures/m above 2000 m depth and only 0.42 fractures/m below this depth, giving an overall average of 0.63 fractures/m (Table 1). In the deeper part of well GPK1, the UBI detected about 1.75 fractures/m between 2850 and 2920 m depth and only

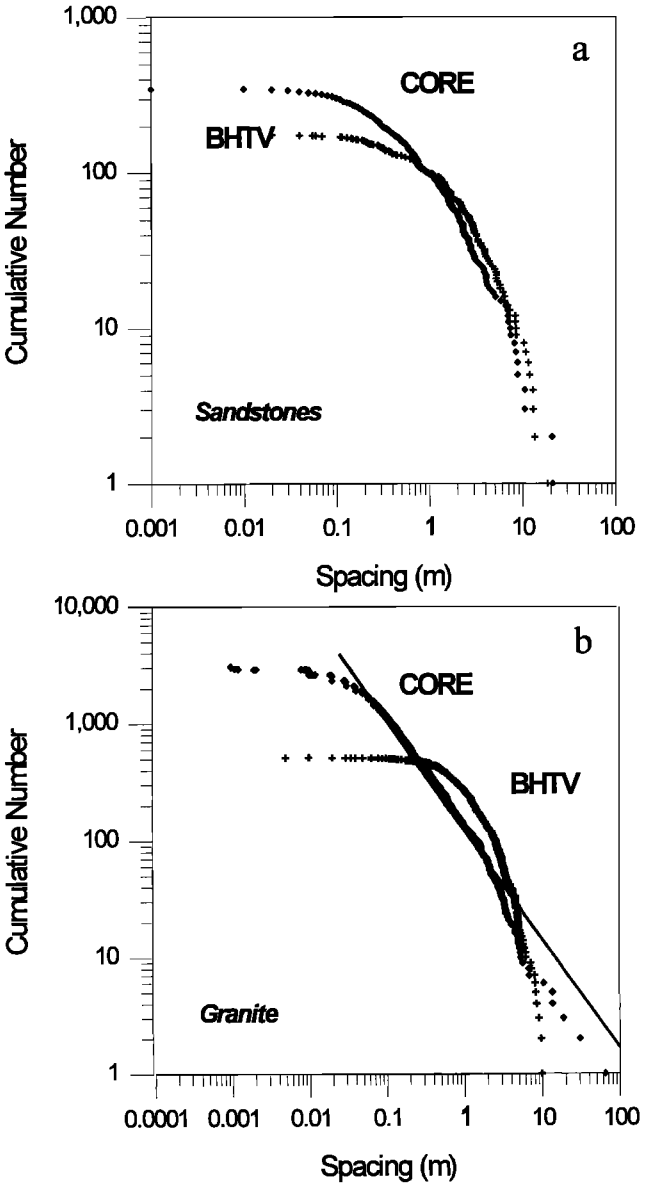

Figure 6. Cumulative distribution of fracture spacing from both core analysis and BHTV (a) in sandstone, and (b) in granite of well EPS1.

0.66 fractures/m below this depth. The lower fracture density (0.33 fractures/m) recorded from ARI images is in agreement with the lower resolution of this tool.

A further comparison made between FMS and core data based on a 50-m-long interval of spot coring in well GPK1 [*Genter et al.*, 1991] resulted in the conclusion that the fracture density defined from the FMS images could be paradoxically higher within intervals of massive granite than within zones of highly fractured and altered granite. For instance, between 1812 and 1814 m depth, about 40 fractures were measured on the core, and only three were recorded from the corresponding FMS image. The underestimation of fractures in such fractured zones can be related to the high conductivity of the clay minerals that not only fill the fractures but also occur in the altered matrix. Consequently, the fractures and their surroundings demonstrate a similar conductive behavior which induces a dark image and prevents the detection of discrete fractures.

Fracture Orientation

The orientation of the fractures defined on the different borehole images within the well GPK1 are shown on Figure 8. The FMS data (1420 to 2000 m depth) show a major near-vertical fracture set trending NNW-SSE (N170° 70°E and N170° 70°W) (Figure 8a). In the deeper part of well GPK1 (2000 to 3600 m), the FMI data show that the major set is now oriented NNE-SSW (N0°-20° 75°W and N10° 75°E) with the westward- dipping fracture set being dominant, as opposed to those in the shallower part of the well (Figure 8b). This change correlates with a decrease in fracture density, which is 2 times lower in the deeper part of the well (Figure 7). The near-vertical fractures sampled by the ARI between 2780 and 3500 m confirm the results of the FMI interpretation, being characterized by a NNE-SSW (N20° 70°W and N20° 70°E) major set and a NW-SE (N140° 60°W and N140° 60°E) minor set (Figure 8c). From 1376 to 2000 m, the BHTV data are compatible with the FMS data showing a major fracture set trending NNW-SSE (N160°-170° 70°W and N160°-170° 70°E) (Figure 8d). However, the

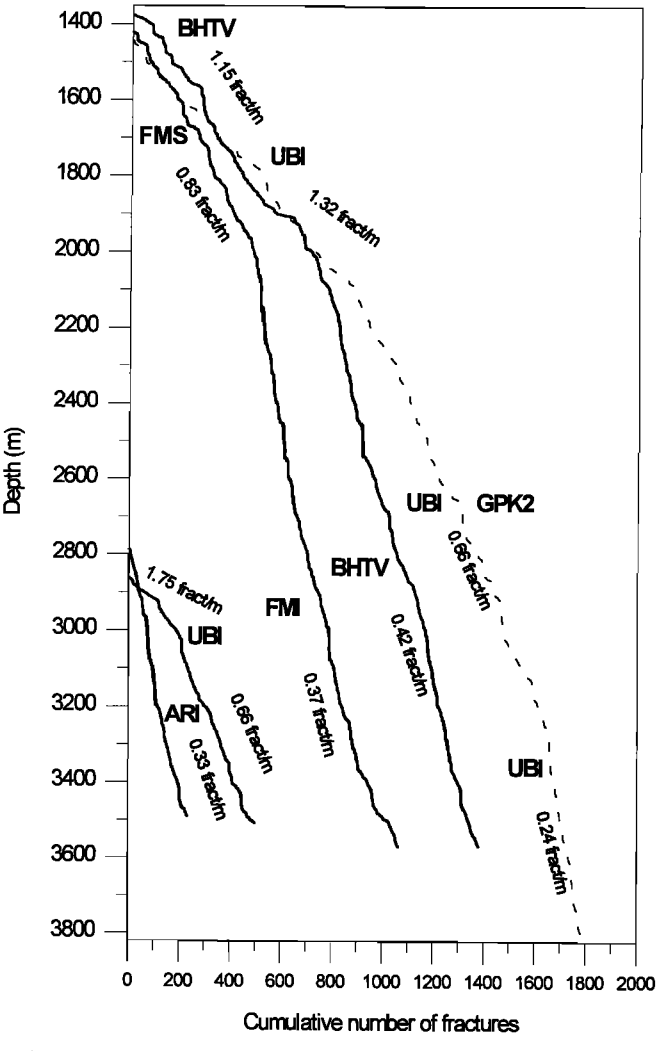

Figure 7. Cumulative number of fractures versus depth collected from electrical and acoustic imagery data over the interval 1376-3800 m in well GPK1 from FMS-4 pads (1420-2000 m), FMI-8 pads (2000-3600 m), ARI (2780-3500 m), BHTV (1376-3600 m), and UBI (2850-3505 m) and in well GPK2 from UBI (1420-3800 m).

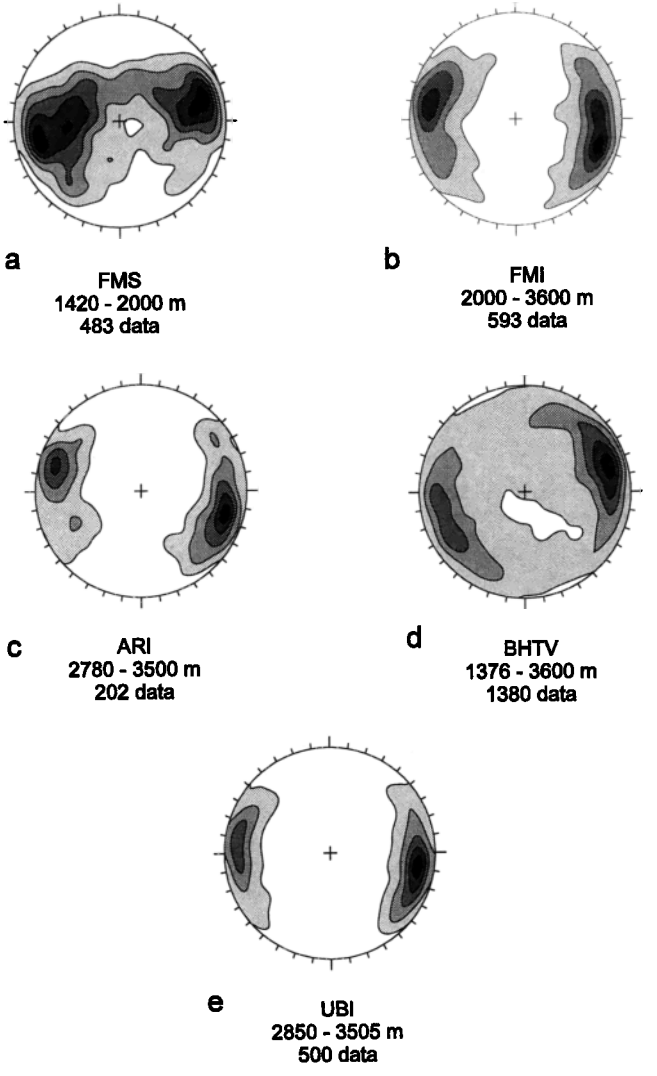

Figure 8. Schmidt isodensity projection (lower- hemisphere) of the pole of natural fractures observed on (a) FMS imagery, (b) FMI imagery, (c) ARI imagery, (d) BHTV imagery, and (e) UBI imagery in well GPK1.

change in orientation of the dominant set in the deeper part of the well (2000 to 3600 m) is not as clear as that given by the FMI results; the BHTV images show several sets with a dominant direction around NNW-SSE (Figure 8d), whereas the FMI gives a major set at NNE-SSW (Figure 8b). The major fracture set sampled by the UBI between 2850 and 3505 m trends NNE-SSW (N10° 75°W and N10° 70°E) which is in close agreement with the FMI results (Figure 8e). Thus in well GPK1, there is a relative stability in the dominant fracture set orientation around NNW-SSE given by the BHTV data but with a high dispersion below 2000 m. In the lower part of the well, the UBI, the FMI, and the ARI tools tend to enhance the NNE-SSW direction.

Fracture Spacing

The BHTV, UBI, FMI, FMS, and ARI data sets obtained in well GPK1 indicate fracture spacings data between 1 cm and 40 m. The fracture-spacing distributions are all rather similar and fit a negative exponential law (Figure 9).

Fracture Determination in Well GPK2

The UBI system was run over the whole granitic section of well GPK2, providing fully oriented images of the borehole wall. About 1800 natural fractures were identified between 1425 and 3800 m depth (Figure 10a). The distributions of the cumulative number of fractures versus depth obtained from the UBI data is plotted on Figure 7 where the curve shows a general fracture density decrease with depth with two changes in the slope. Thus three main sections could be distinguished in well GPK2. The UBI collected about 1.35 fractures/m from 1425 to 2100 m, 0.66 fractures/m from 2100 to 3100 m, and 0.27 fractures/m from 3100 to 3800 m. The major near-vertical fracture set trends N-S to NNW-SSE (N0° 70°W and N160° 70°E) (Figure 10b). A main open fault located at 2115 m depth, and which caused total mud loss during the drilling, is oriented N150° and dips to the east. The cumulative fracture spacing distribution derived from the UBI (Figure 9) approximately follows a negative exponential law; the fracture-spacing data range between 1 mm and 60 m.

Discussion

One- dimensional fracture characterization depends on the fracture-sampling resolution (truncation effect). With very fine resolution sampling, such as core data, the truncation effect is minimal. An ideal fracture core sampling should be done with a binocular or a microscope, but this does not correspond to a pragmatic approach. With borehole imaging data, the resolution is coarser than with core data and is related to the tool configuration. At Soultz, it has been found that the smallest fractures are not sampled (less than 1 mm thick) and that closed or sealed fractures are misimaged: open fractures (BHTV and UBI) or conductive fractures (FMI, FMS, and ARI) are detected preferentially. Owing to these limitations, we find that fracture density, cluster detection, and fracture spacing are missampled.

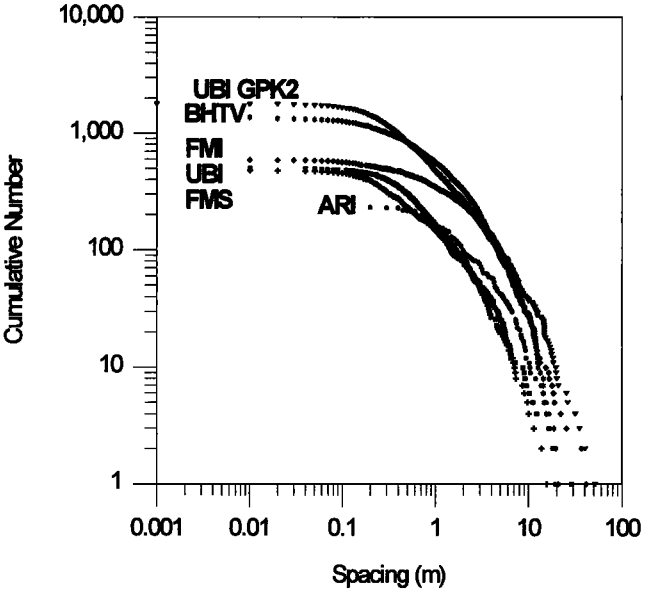

Figure 9. Cumulative distribution of fracture spacing from BHTV, FMI, FMS, ARI, and UBI analyses in the granitic section of wells GPK1 and GPK2.

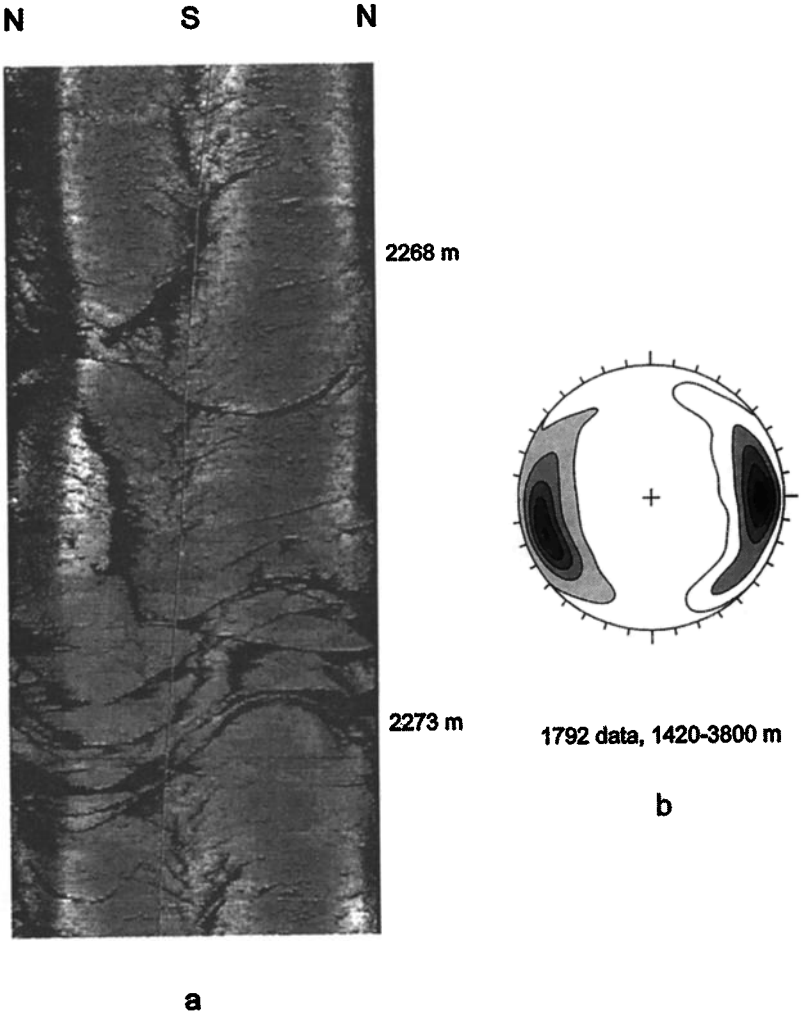

Figure 10. (a) Example of an UBI image showing many discrete fractures and (b) a Schmidt isodensity projection (lower- hemisphere) of the pole of natural fractures collected in well GPK2.

The resolution problems preferentially act on the fracture spacing distribution. From cumulative fracture-spacing distribution, it is possible to obtain the maximum spacing value between two consecutive fractures. The observed fracture spacing of core data in granite has a good fit with a power law distribution with a slope of -0.94 (Figure 6b). The spacing population corresponding to BHTV data evolves into a negative exponential law, reflecting the degrading process related to imagery resolution which transforms the power law into an exponential law (Figure 6b). Moreover, the highest spacing values are 10 m with the exponential law and are over 100 m with the power law (Figure 6b). Concerning the BHTV, FMI, FMS, ARI and UBI data, the fracture-spacing distributions fit a negative exponential law, and the maximum spacing values obtained from these distributions range between 15 and 50 m (Figure 9).

In the sandstone, both the core and the BHTV fracture-spacing distributions tend to a maximum of 10 m (Figure 6a). Even though some fracture- clusters occur in the cored sandstone, it was not possible to correlate fracture spacings with a power law as in the cored granite. Since the distributions of fracture spacings determined from the core and the BHTV follow approximately the same law for spacing values >0.8 m (Figure 6a), the spatial organization of the fractures in the sandstone could be strongly influenced by the occurrences of adjacent sedimentological beds acting as surface discontinuities. As it has been mentioned by many authors [*Ladeira and Price*, 1981; *Huang and Angelier*, 1989], fracture spacing is related to bed thickness. The power law distribution of fracture spacings observed in the cored granite indicates that the fractures are clustered throughout the well (Figure 6b). This result was already well known from the core examination [*Genter and Traineau*, 1992] and by application of the Dust Cantor method on the fracture database [*Ledesert et al.*, 1993]. This means that some depths show a high frequency of low-spacing values within a cluster and other depths show a low frequency of high-spacing values between clusters. In well EPS1, the fracture-spacing distribution determined from the BHTV analysis for the granite is exponential and may not be the actual fracture distribution (Figure 6a). The resolution problems are minimal with the UBI system since this tool gives the highest fracture-density values and the maximal fracture-spacing values (Figures 7 and 9).

One-dimensional fracture sampling has its limitations where quantifying the geometry of a fracture system is concerned. As core sampling and high-resolution borehole imag-

ing tools only image the borehole wall, there is no actual penetration into the formation; an exception is the low-resolution ARI tool. With structural data obtained from borehole analysis, it is difficult to determine how far a fracture extends away from the well and thus the nature of its three-dimensional far-field fracture geometry. The problem is how can we use single-well information to extrapolate to the reservoir scale? The significance of fracture orientation (strike and dip) of a given fracture which is sampled along the borehole axis, but which may extend away from the well, must be considered with care. Nevertheless, the data collected within the different Soultz wells indicate that the dominant almost N-S fracture set orientation is persistent: a stable fracture orientation that could possibly be related to the rifting activity of the Rhine graben during Cenozoic times. Locally, the persistence is not very good (e.g., the BHTV data in well EPS1); it can be related to the occurrence of induced fractures, especially as these are difficult to separate clearly from naturally formed fractures. Thus core sampling or high-resolution imaging techniques are not adapted to obtain structural information away from the borehole wall; this is better done with a low-resolution imaging tool such as ARI.

Fracture characterization at Soultz based on a comparison between televiewer and core data becomes difficult in the intensely fractured zones. Multiple intersecting fractures occur, and it becomes problematic to reconstruct a one to one relationship between an imagery log and a core [*Paillet et al.*, 1985].

Conclusion

Detailed studies of small-scale fracture distributions were carried out in three deep HDR wells (EPS1, GPK1, and GPK2) located at Soultz-sous-Forêts (Rhine graben, France). The study of the density and spatial orientation of the fractures was based on coring and high-resolution borehole imaging techniques.

In the fully cored EPS1 well (1000-2230 m total depth), the fracture population in both sandstone and granite was analyzed in one dimension through well data (core and acoustic borehole televiewer (BHTV)) in terms of fracture density, orientation, and spacing. In the sandstone, BHTV detected about 50% of the fracture population observed on the cores, whereas in the granite only 500 fractures were sampled by the BHTV, compared to 3000 fractures observed on the cores. Owing to its spatial resolution, the BHTV was not able to detect fractures thinner than 1 mm, which represent 75% of the entire natural fracture population on the cores. Furthermore, the BHTV was not able to properly characterize the very closely spaced fractures and thus their clustered organization, observed on the core sections. Nevertheless, the spatial orientation of the fractures was correctly sampled since the BHTV distinguished the main fracture sets. The spatial organization of individual fractures collected in one dimension at Soultz is strongly dependent on the fracture sampling resolution. In the granitic section of well EPS1, the fracture-spacing distributions collected on core data (fine resolution) and on BHTV data (coarse resolution) show a power law and a negative exponential law, respectively.

In the uncored GPK1 and GPK2 wells, the fracture system was only investigated by means of different electrical and acoustic imagery techniques from 1400 to 3800 m depth. Two different borehole sections were evidenced in terms of fracture density: an upper, highly fractured section from 1400 to 2000 m and a deeper, poorly fractured section from 2000 to 3800 m. The dominant fracture sets trend NNE-SSW and NNW-SSE and are very close to those evidenced in well EPS1.

Acknowledgments. This research has been carried out within the framework of the European Hot Dry Rock Project funded by the Commission of the European Communities (DG XII). Geological investigations were supported by the scientific research programme of BRGM (project S07). The authors are grateful to the coordinating organization, Socomine, which provided samples, borehole data, and helpful assistance on site. The English of the final version of the manuscript was improved by Patrick Skipwith, BRGM Translation Service. The manuscript has greatly benefited from the constructive comments of Colleen Barton, François Cornet, and Bezalel Haimson.

References

Baria, R., J. Garnish, J. Baumgärtner, A. Gérard, and R. Jung, Recent developments in the European HDR research programme at Soultz-sous-Forêts (France), paper presented at *World Geothermal Congress*, ENEL, Florence, Italy, May 18-31, 1995.

Barton, C.A., and M.D. Zoback, Self-similar distribution and properties of macroscopic fractures at depth in crystalline rock in the Cajon Pass scientific drill hole, *J. Geophys. Res., 97*, 5181-5200, 1992.

Barton, C.A., L. Tesler, and M.D. Zoback, Interactive image analysis of Borehole Televiewer data, in *Automated Pattern Analysis in Petroleum Exploration*, edited by I. Palaz and S.K. Sengupta, pp. 265-284, New York, Springer-Verlag, 1991.

Benderitter, Y., A. Tabbagh, and P. Elsass, Calcul de l'effet thermique d'une remontée hydrothermale dans un socle fracturé. Application à l'anomalie géothermique de Soultz-sous-Forêts (Nord Alsace), *Bull. Soc. Géol. Fr., 166*, 37-48, 1995.

Bourke, L.T., Sedimentological borehole image analysis in clastic rocks: A systematic approach to interpretation, in *Geological Applications of Wireline Logs II*, Geol. Soc. *Spec. Publ. London, 65*, 31-42, 1992.

Bourke, L.T., P. Delfiner, J.-C. Trouiller, T. Fett, M. Grace, S. Luthi, O. Serra, and E. Standen, Using Formation MicroScanner images, *Techn. Rev., 37*, 16-40, 1989.

Boyeldieu, C., and P. Jeffreys, Formation MicroScanner: New developments, paper presented at 11th European Evaluation Symposium, Soc. of Prof. Well Log Anal., Oslo, 1988.

Brun, J.P., F. Wenzel, and Ecors-Dekorp seismic teams, Crustal-scale structure of the southern Rhine Graben from Ecors-Dekorp seismic reflection data, *Geology, 19*, 758-762, 1991.

Brun, J.P., M.A. Gutscher, and Dekorp-Ecors teams, Deep crustal structure of the Rhine Graben from Dekorp-Ecors seismic reflection data: A summary, *Tectonophysics, 208*, 139-147, 1992.

Davies, D.H., et al., Azimuthal resistivity imaging: A new generation laterolog, SPE Paper 24676 presented at 1992 SPE Annual Technical Conference, Soc. of Petr. Eng., Washington D.C., 1992.

Dezayes, C., T. Villemin, A. Genter, H. Traineau, and J. Angelier, Analysis of fractures in boreholes of the Hot Dry Rock project at Soultz-sous-Forêts (Rhine graben, France), *Sci. Drill., 5*, 31-41, 1995.

Ekstrom, M.P., C.A. Dahan, M.Y. Chen, P.M. Lloyd, and D.J. Rossi, Formation imaging with microelectrical scanning arrays, *Trans SPWLA, Annu. Logging Symp., 27th*, 21pp., 1986.

Elsass, P., L. Aquilina, A. Beauce, Y. Benderitter, H. Fabriol, A. Genter, and H. Pauwels, Deep structures of the Soultz-sous-Forêts HDR site (Alsace, France), paper presented at *World Geothermal Congress*, ENEL, Florence, Italy, May 18-31, 1995.

Engelder, T., Joints and shear fractures in rock, *Fracture Mechanics of Rock*, edited by K. Atkinson, pp. 27-69, Academic, San Diego, Calif., 1987.

Faivre, O., Fracture evaluation from quantitative azimuthal resistivities, SPE paper 26434 presented at 1993 SPE Annual Technical Conference, Soc. of Petr. Eng., Houston, Texas, 1993.

Flores, E.L., and J.J. Royer, Convective heat transfert around the Soultz-sous-Forêts geothermal site (Rhine graben), in *Proceedings of the VIth International Symposium, Continental Scientific Drilling Programs, Doc. B.R.G.M., 223*, 155-170, 1992.

Garnish, J., R. Baria, J. Baumgartner, and A. Gérard, The European Hot Dry Rock programme 1994-1995, *Trans. Geotherm. Resour. Counc., 18*, 431-438, 1994.

Genter, A., and D. Genoux-Lubain, Evaluation de la fracturation dans le forage GPK1 à partir de l'imagerie ARI entre 2780m et 3500m (Soultz-sous- Forêts, France), *Open File Rep. R 38099*, 14pp., Bur. de Rech. Géol. et Minières, Orléans, France, 1994.

Genter, A., and H. Traineau, Borehole EPS-1, Alsace, France: Preliminary geological results from granite core analyses for Hot Dry Rock research, *Sci. Drill., 3*, 205-214, 1992.

Genter, A., and H. Traineau, Analysis of macroscopic fractures in granite in the HDR geothermal EPS-1 well, Soultz-sous-Forêts (France), *J. Volcanol. Geotherm. Res., 72*, 121-141, 1996.

Genter, A., P. Martin, and P. Montaggioni, Application of FMS and BHTV tools for evaluation of natural fractures in the Soultz geothermal borehole GPK1, *Geotherm. Sci. Tech., 3*, 69-82, 1991.

Genter, A., H. Traineau, C. Dezayes, P. Elsass, B. Ledesert, A. Meunier, and T. Villemin, Fracture analysis and reservoir characterization of the granitic basement in the HDR Soultz project (France), *Geotherm. Sci. Tech., 4*, 189-214, 1995.

Genter, A., C. Castaing, G. Courrioux, C. Dezayes, P. Elsass, Y. Halbwachs, H. Tenzer, H. Traineau, and T. Villemin, Multiscale organisation of fractures in the HDR Soultz granite reservoir from core and borehole-imaging data, paper presented at *3rd International HDR Forum*, GRC, Santa Fe, N. M., May 13-16, 1996.

Gillespie, P.A., C.B. Howard, J.J. Walsh, and J. Watterson, Measurement and characterisation of spatial distributions of fractures, *Tectonophysics, 226*, 113-141, 1993.

Huang, Q., and J. Angelier, Fracture spacing and its relation to bed thickness, *Geol. Mag., 126* (4), 335-362, 1989.

Jung, R., J. Willis-Richard, J. Nicholls, A. Bertozzi, and B. Heinemann, Evaluation of hydraulic tests at Soultz-sous-Forêts, European HDR-site, paper presented at *World Geothermal Congress*, ENEL, Florence, Italy, May 18-31 1995.

Kappelmeyer, O., A. Gérard, W. Schloemer, R. Ferrandes, F. Rummel, and Y. Benderitter, European HDR project at Soultz-sous-Forêts general presentation, *Geotherm. Sci. Tech., 2*, 263-289, 1991.

Ladeira, F.L., and N.J. Price, Relationship between fracture spacing and bed thickness, *J. Struct. Geol., 3*, 179-183, 1981.

Le Carlier, C., J.J. Royer, and E.L. Flores, Convective heat transfer at Soultz-sous-Forêts geothermal site. Implications for oil potential, *First Break, 12*, 553-560, 1994.

Ledesert, B., J. Dubois, A. Genter, and A. Meunier, Fractal analysis of fracture applied to Soultz-sous-Forêts Hot Dry Rock geothermal program, *J. Volcanol. Geotherm. Res., 57*, 1-17, 1993.

Luthi, S.M, and J.R. Banavar, Application of borehole images to three-dimensional geometric modeling of eolian sandstone reservoirs, Permian Rotliegende, North Sea, *Geol. Soc. Am. Bull, 72*, 1074-1089, 1988.

MacLeod, C.J., S. Allerton, I.G. Gass, and C. Xenophontos, Structure of a fossil ridge transform intersection in the Troodos ophiolite, *Nature, 348*, 717-720, 1990.

Paillet, F.L., W.S. Key, and A.E. Hess, Effects of lithology on televiewer-log quality and fracture interpretation, paper presented at 26th annual logging Symposium, Soc. of Prof. Well Log Anal., Dallas, Tex., June 17-20, 1985.

Pezard, P.A., R.N. Hiscott, M.A. Lovell, A. Collela, and A. Malinverno, Evolution of the Izu-Bonin intraoceanic forearc basin, western Pacific, from cores and FMS images, in *Geological Applications of Wireline Logs II, Geol. Soc. Spec. Publ. London, 65*, 43-69, 1992.

Pollard, D.D., and A. Aydin, Progress in understanding jointing over the past century, *Geol. Soc. Am. Bull., 100*, 1181-1204, 1988.

Schellschmidt, R., and R. Schulz, Hydrothermic studies in the Hot Dry Rock project at Soultz-sous-Forêts, *Geotherm. Sci. Tech., 3*, 217-238, 1991.

Schlumberger, Dipmeter interpretation, in *Fundamentals*, Schlumberger, New York, 1986.

Schlumberger, FMI, full formation microimager, *Rep. SMP 9210*, 42 pp., Houston, Tex., 1992.

Schlumberger, Ultrasonic imaging, *Rep. SMP-9230*, 28 pp., Houston, Tex., 1993.

Tenzer, H., L. Mastin, and H. Heinemann, Determination of planar discontinuities and borehole geometry in the crystalline rock of borehole GPK-1 at Soultz-sous-Forêts, *Geotherm. Sci. Tech., 3*, 31-67, 1991.

Tenzer, H., P. Budeus, and R. Schellschmidt, Fracture analyses in Hot Dry Rock drillholes at Soultz and Urach by borehole televiewer measurements, *Trans. Geotherm. Resour. Counc., 16*, 317-321, 1992.

Wenzel, F., J.P. Brun, and the Ecors-Dekorp working group, A deep reflection seismic line across the Northern Rhine Graben, *Earth Planet. Sci. Lett., 104*, 140-150, 1991.

Zemanek, J., E. E. Glenn, L.J. Norton, and R.L. Caldwell, Formation evaluation by inspection with the borehole televiewer, *Geophysics, 35*, 254-269, 1970.

Ziegler, P.A., European Cenozoic rift system: Case history studies on rifts: European and Asian, *Tectonophysics, 208*, 91-111, 1992.

C. Castaing, A. Genter, and H. Traineau, Département Géophysique et Imagerie Géologique, Direction de la Recherche, Bureau de Recherches Géologiques et Minières, 3 avenue Claude Guillemin, BP 6009, F-45060 Orléans Cedex 2, France. (e-mail: a.genter@brgm.fr)

C. Dezayes and T. Villemin, Laboratoire Géodynamique des Chaînes Alpines, Université de Savoie, F-73376 Le Bourget de Lac, France.

H. Tenzer, Stadtwerke Bad Urach, Markplatz 8-9, D-72574 Bad Urach, Germany.

(Received July 12, 1996; revised February 15, 1997;
accepted February 24, 1997.)